The Use of Computational Fluid Dynamics in Predicting the Tidal Flushing of Animal Burrows

S. F. Heron and P. V. Ridd[a]

Marine Geophysical Laboratory, School of Mathematical and Physical Sciences, James Cook University, Townsville QLD 4811, Australia

Numerical hydrodynamic modelling has been used extensively over the last few decades to simulate flow in the ocean, bays and estuaries; however, modelling of much smaller scale phenomena is less common. In this work a commercially available Computational Fluid Dynamics package (FIDAP), normally used for industrial applications, was used to simulate tidally-induced flow in multi-opening animal burrows. U-shaped burrows of varying complexities were modelled to determine the effect of different surface characteristics and burrow geometries on surface water velocities, burrow velocities and burrow flushing times. The turbulent 2D model showed the slope of the surface water was proportional to the square of both the surface and burrow velocities. The effect of placing a root in the surface flow was to reduce the surface water velocity; however, the burrow flow depended upon the root position. For the root location either upstream or downstream of the burrow, the burrow velocity was reduced by 50%. With the root located between the burrow openings the burrow velocity increased by 200%, due to the increase in pressure difference across the burrow openings. A buttress root placed in the flow immediately downstream of the upstream burrow, caused the burrow flushing rate to increase significantly with increasing buttress height. Flushing times for burrows of varying depth were determined computationally by use of a tracer for the burrow water. For a burrow of depth 1·2 m, the flushing times were 5 and 28 min for root location between the burrow openings and downstream of the burrow, respectively. Animal burrows often consist of multiply-connected loops. A second burrow was added to the primary burrow and flushing times were found to be 15 and 38 min, respectively. A burrow system of four connected burrows was modelled which had corresponding flushing times up to 24 and 47 min, respectively. The calculated times are consistent with the hypothesis that a significant flushing of animal burrows occurs within a single tidal event. This preliminary investigation indicates that CFD models may be very useful in studying small scale hydrodynamic phenomena such as flow in animal burrows.

© 2001 Academic Press

Keywords: burrows; computer simulation; flushing time

Introduction

Numerical models of geophysical fluids have provided insight into various phenomena at the scale of oceans, bays and estuaries (Furukawa *et al.*, 1997; Wolanski & Ridd, 1986; Bode *et al.*, 1997). Small scale hydrodynamic modelling is much less common. The Fluid Dynamics Analysis Package (FIDAP) is one example of commercial packages that are primarily used to model processes in industrial applications. These packages may be used to simulate flows in biophysical applications, specifically in this work, the flushing flow of animals burrows.

Animal burrows are located in a variety of marine and freshwater environments. These burrows play a role in many exchange processes in the banks and beds of freshwater lakes and rivers, and coastal and estuarine regions. Irrigation and flushing of the burrows provides a mechanism that can enhance the exchange of materials between the surface water and sediment. Such materials may include salt, nutrients, oxygen and pollutants.

Flow in animal burrows has received increased attention by researchers in recent years (Webster, 1992; Ridd, 1996). The study of Allanson *et al.* (1992) investigated flow through burrows of the thalassinidean prawn, *Upogebia africana* Ortmann. These burrows are found only in lowtide mud banks of open estuaries and sheltered bays, and are absent from areas of little tidal activity. The burrow shape was simplified as a U-tube shape with a volcano-shaped mound at one burrow opening. As the surface flow passes over the mound, it creates a pressure difference between the burrow openings and thus induces flow through the burrow. An analytical approach was undertaken by Allanson *et al.* (1992) and experimental comparisons were made using a laboratory

[a]Corresponding author.

constructed simulation of such a burrow. Using surface currents in the range 5–17 cm s^{-1} the residence time of a dye tracer was measured, from the entry to the tube until the central streak first emerged. These times were measured in the range 0·2–1·0 s and, using the tube length, the maximum discharge velocity from the U-tube was calculated. Allanson et al. (1992) showed there was a linear relationship between the free surface velocity and the mean discharge velocity from the burrow.

One environment with an abundance of massive burrow networks is that of mangrove swamps (Ridd, 1996). Mangrove ecologies are characterized by their ability to exist in soils that are highly impermeable to water flow. The impermeability of the mangrove sediment causes difficulty in the exchange of solutes between the subsurface mangrove roots and the surface water. In mangrove areas, the transport of salt is of great importance. Salt is excluded by the roots and diffusion from the root zone is essential to avoid fatal hypersaline conditions (Passioura et al., 1992). The diffusion through the sediment is impeded by the impermeability of the soil. In sediment without burrows, salt must be diffused from root to subrace water, whereas with burrows the diffusion distance from root to burrow water is much shorter. The diffusion coefficient in mangrove swamp sediment was calculated by Hollins et al. (1999) to be $4·6 \times 10^{-5}$ m^2 day^{-1}. With the presence of burrows in the mangrove soil, the diffusion distance, and thus time, from root to water is greatly decreased. This shorter distance over which slow diffusion processes occur, speeds the removal of salt provided that burrows are occasionally flushed.

Water flow through animal burrows during the tidal cycle completes the transport of salt to the surface water. Ridd (1996), Stieglitz et al. (2000b) and Hollins and Ridd (submitted) have shown that salt is flushed with the burrow water by any tide that is sufficiently high to inundate the ground surface at the burrow openings. Mangrove forests are found within the inter-tidal zone; however, while some regions will be regularly inundated others may only be inundated during the highest of spring tides. Mangroves at these ecological limits are stunted in their growth due to the increasing stress of high salt concentration (Tomlinson, 1986), which may be partially attributed to poor flushing of animal burrows.

The flushing of burrows may occur due to the tidal water slope across the burrow openings that causes a pressure difference between the openings. The magnitude of the water slope can reach as much as 10^{-3} (Aucan & Ridd, 2000), corresponding to a pressure gradient of approximately 10 Pa m^{-1}. The water gradient only reaches this magnitude in the initial (flood) and final (ebb) stages of the high tide inundation and generally remains around the value 10^{-4} (Aucan, pers. comm.). The pressure difference across the burrow openings drives a flow through the burrow in the same direction as the surface current (Ridd, 1996). The surface currents during a tidal cycle have been observed to be as high as 15 to 20 cm s^{-1} on both flood and ebb tides, and are more commonly found in the range of 5–10 cm s^{-1} (Furukawa et al., 1997; Wolanski et al., 1992).

Webster (1992) showed that the presence of waves in the surface water leads to oscillatory motion within empty burrows. This motion is driven by the different water levels at the openings of two-opening burrows. Higher water level (higher pressure) at the upstream opening dives the burrow flow in the same direction as the surface flow. As the wave passes over the burrow, there is higher pressure at the downstream opening, thus driving the burrow flow in the opposite direction. This oscillation effect continues with wave propagation and considerably enhances the solute dispersion by turbulent diffusion. Webster's work showed that solute dispersion rates due to the oscillatory motion were much greater (e.g. 26 times for O$_2$) than by molecular diffusion alone.

There is some variation in results of measurements of the efficiency of this flushing process in mangrove swamps. Stieglitz et al. (2000b) has suggested that there is complete flushing of burrow water in approximately 1 h, i.e. within the time span of a single tidal event. This study was performed by replacing the burrow water with a sugar solution of similar density and measuring the variation in conductivity as the solution was replaced with (higher conductivity) surface water. On the other hand, Hollins and Ridd (submitted) measured that the quantity of water moving into a burrow during one tidal cycle was of the order of 30% of the burrow volume. This work was performed by using a rhodamine dye tracer to mark the burrow water prior to the tidal event and then measuring the relative fluorescence over the tidal period to determine the mixing rate. A second method used by Hollins and Ridd involved measurements of the oxygen concentration of the ground water. Accounting for oxygen diffusion from mangrove roots and microbial oxygen consumption, the increased values of oxygen concentration due to the inflow of oxygenated surface water were significant and suggested that approximately one third of the burrow volume was flushed each tidal cycle, consistent with the dye experiment. Although there is some variance between the results of Stieglitz et al. (2000b)

and Hollins and Ridd (submitted), in both cases significant flushing was observed.

This work provides a numerical investigation into the pressure-induced (tidal) flow through empty animal burrows. Any irrigation by the resident animals in the burrow is not investigated in this study. Initially the laboratory study of Allanson *et al.* (1992) is replicated numerically to validate the techniques. Simulations of various burrow geometries are undertaken to investigate the effects of surface water slope, surface water obstructions, burrow depth and multiple burrow systems. Velocities throughout the flow domain, and the time required to completely flush the burrow water are determined for the various geometries.

Methods

The tidal flushing was modelled in two dimensions using the Fluid Dynamics Analysis Package, FIDAP. This package uses the finite element method to solve the isothermal Navier-Stokes equations (Fluid Dynamics International, 1993):

Continuity:
$$\frac{\partial \rho}{\partial t} + \nabla \rho \boldsymbol{u} = 0$$

Momentum: $\rho \left(\dfrac{\partial \boldsymbol{u}}{\partial t} + \boldsymbol{u} \nabla \boldsymbol{u} \right) = - \nabla p + \nabla \tau - \rho \boldsymbol{g} \sum_n \beta_c c + \rho \boldsymbol{f}$

Transient + Convective = Pressure + Viscous − Buoyancy + Body Force

where the symbolism is as follows: ρ=density; t=time; u=velocity; ∇=gradient operator; p=pressure; τ=stress tensor; g=gravity; c=species concentration; β_c=species volume expansion coefficients; f=body force.

The effects of turbulence were modelled using a two-equation k-ε model, where k is the turbulent kinetic energy and ε is the viscous dissipation rate of the turbulent kinetic energy. The transport equations for these turbulent quantities are solved according to

$$\rho \left(\frac{\partial k}{\partial t} + \boldsymbol{u} \nabla k \right) = \nabla \left(\frac{\mu_t}{\sigma_k} \nabla k \right) + \mu_t \Phi + \mu_t \frac{\beta_c}{S_t} \boldsymbol{g} \nabla c - \rho \varepsilon$$

$$\rho \left(\frac{\partial \varepsilon}{\partial t} + \boldsymbol{u} \nabla \varepsilon \right) = \nabla \left(\frac{\mu_t}{\sigma_\varepsilon} \nabla \varepsilon \right) + c_1 \frac{\varepsilon}{k} \mu_t \Phi$$
$$+ c_1 (1 - c_3) \frac{\varepsilon}{k} \mu_t \frac{\beta_c}{S_t} \boldsymbol{g} \nabla c - \rho c_2 \frac{\varepsilon^2}{k}$$

where $\mu_t = \rho c_\mu \dfrac{k^2}{\varepsilon}$ is the turbulent viscosity; $\mu_t \Phi$ is the turbulent viscous dissipation and the model constants

are recommended by FIDAP for isothermal flows (Fluid Dynamics International, 1993) to be:

$$c_\mu = 0{\cdot}09, \ \sigma_k = 1{\cdot}00, \ \sigma_\varepsilon = 1{\cdot}30, \ c_1 = 1{\cdot}44, \ c_2 = 1{\cdot}92,$$
$$c_3 = 0{\cdot}8, \ S_t = 0{\cdot}9.$$

The velocity and turbulence profiles were solved using a steady-state analysis and constant density was assumed throughout the domain.

The velocity and turbulence fields are independent of the concentration and thus are constant in time, so the equations may be solved consecutively. The burrow flushing time for each geometry was determined by ' colouring ' the burrow with a tracer and using an advection-diffusion analysis. This process accepts the steady-state profiles as input and then solves the time-dependent tracer equation (tracer n):

$$\rho \left(\frac{\partial c_n}{\partial t} + \boldsymbol{u} \nabla c_n \right) = \rho \nabla (\alpha_n \nabla c_n) + q_{c_n} + R_n$$

Transient + Convective = Diffusive + Source + Reaction

where: c_n=tracer concentration; α_n=molecular diffusivity; q_{c_n}=*source term;* R_n=chemical reaction rate. For the present analysis, the source and reaction terms are removed; however, these could be retained for analyses investigating oxygen concentration.

The boundary condition which drives the flow was defined by the water surface slope across the flow domain. The pressure difference due to the slope was calculated over the length of the flow domain. This pressure difference was simulated by defining a flow-directed boundary stress at the inflow of the surface water. This stress combines the effects of pressure and variation of velocity in the flow direction. The inflow stress condition produced the required pressure difference across the domain and an appropriate vertical velocity profile for the surface water. The variation in the effective surface water level across the flow domain was adjusted to the order of 0·1–1%. The vertical component of velocity at the top, inflow and outflow of the surface water were set to zero, as was the total velocity at the ground surface.

The surface of the swamp is characterized in the model using a roughness length parameter. The roughness parameter of the swamp sediment was modified so as to produce appropriate velocities for the surface flow, as constrained by the required slope-induced pressure gradient. The surface flow in mangrove swamps is also greatly affected by the presence of surface roots and other obstructions, e.g. stilt roots in *Rhizophora* spp. and pneumatophores in *Avicennia* spp. The friction to the flow caused by these

obstructions was too large to be implicitly simulated by the simple use of the roughness parameter (while maintaining convergence criteria). For this reason roots were added explicitly to the model domain to better represent the swamp conditions.

One further example of these obstructions, observed in *Ceriops tagal* forests in North Queensland, is the buttress root of the mangrove trees. The interesting point regarding flow in animal burrows is that the upstream burrow opening is often located near to, and upstream of, the buttress root. The effect of the buttress near the burrow opening on the flushing rate was investigated using this model.

The burrow shapes in mangrove swamps are complex structures with multiple openings to each chamber. The burrows may be constructed of many loops reaching to depths of 1·2 m (Stieglitz *et al.*, 2000*a*). For this 2D analysis we have simplified the burrow geometry to a single loop with two surface openings. The simplified geometry has the same general shape of observed animal burrows. In a similar manner as for the ground surface, a roughness parameter is assigned to the burrow walls. This roughness mimics the effect of the random wall deviation on the flow.

Multiple burrow loops are added at a later stage, to simulate the more complex burrows constructed by a wider range of animal species (e.g. *Sesarma messa*, *Alpheus* cf *macklay*). While the geometry of these burrows seems somewhat simplified from actual burrows, it is a suitable 2D representation of these deeper burrows for the purpose of simulating the tidal flushing dynamics. It is impossible to exactly replicate the geometry of a particular animal burrow, and also impractical as any given burrow would be different from all other burrows. Thus, in order to simulate flows in burrows, it is important to concentrate on the main hydrodynamic processes that control the flow; in this case the approximate parameters of the water motion and burrow geometry. The flow characteristics, and the general burrow shape and dimensions, are consistent with observations. The detail of individual burrows will likely have a small influence on the flushing, however the overall flushing characteristics will be consistent. Hence we can be confident that the simulation will provide a good representation of burrow flushing.

Results

U-tube burrows, Upogebia africana Ortmann

The experiments of Allanson *et al.* (1992) were simulated using the boundary stress condition at the inflow of the surface water. The parameters were set as per
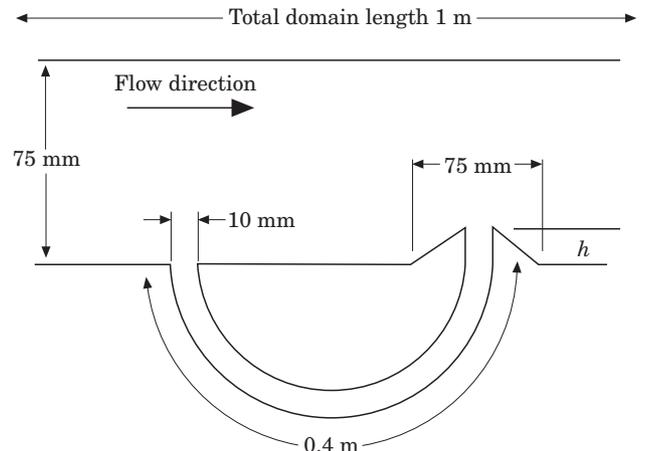
FIGURE 1. Geometry of flow domain used by Allanson *et al.* (1992)
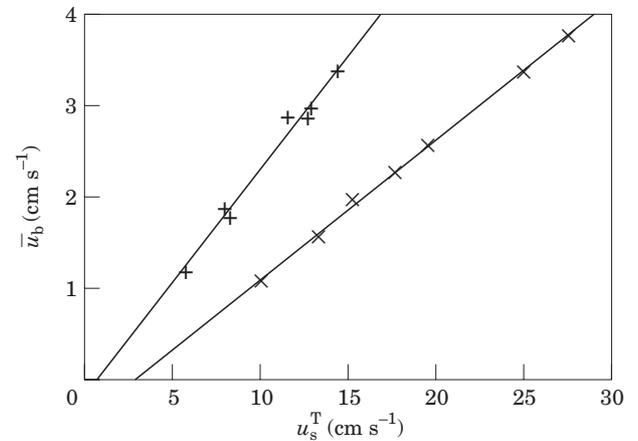
FIGURE 2. The regression of mean burrow velocity from the burrow upon inflow surface velocity. × : 10 mm; + : 20 mm.

those from the experimental investigation of Allanson *et al.* (1992) and the flow domain is shown in Figure 1: surface water length 1 m and depth 75 mm; burrow length 0·4 m and diameter 10 mm; simple volcano-shaped mounds located at burrow output; base diameter 75 mm; height, h=10 mm and 20 mm.

Figure 2 shows the relationship between the water velocity at the top of the surface, u_s^T, and the mean discharge velocity of the burrow, $\overline{u}_b$. The linear relation reported by Allanson *et al.* (1992) is duplicated by the model. The gradients of the lines in Figure 2 are 0·152 and 0·247 for 10 mm and 20 mm mounds, respectively. These values are approximately 125% and 160% of the gradients reported by Allanson *et al.* (1992). This variation may be due to different roughness characteristics between the model and experiment or the smaller influence of the surface roughness in the burrow due to the 2D geometry of

(a)

(b)

(c)

(d)
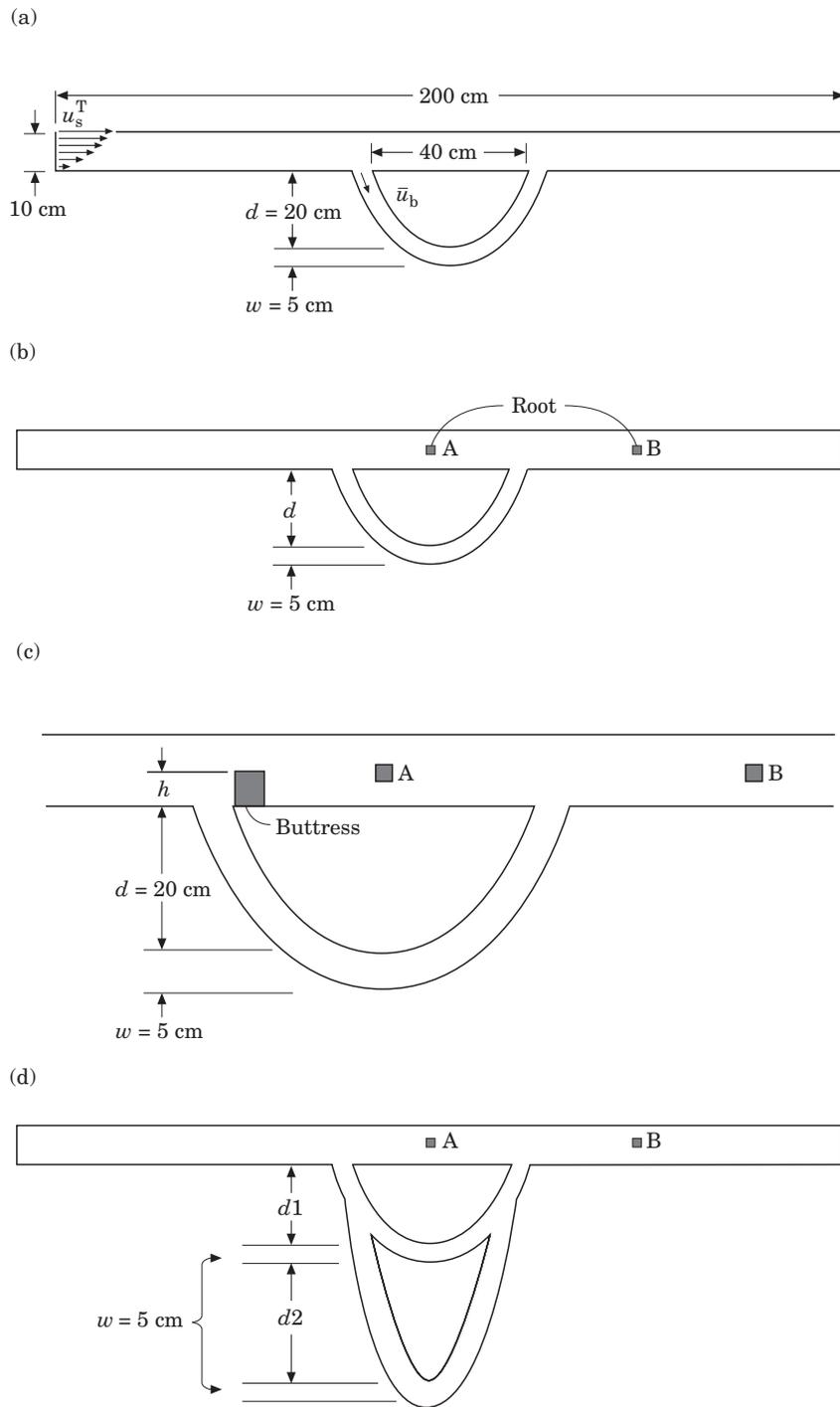
FIGURE 3 (a)–(d)

the model. This validation indicates the numerical techniques developed here are in broad agreement with the experimental data of Allanson *et al*. (1992).

Burrows in mangrove swamps

The numerical model was used to simulate flows through animal burrows in mangrove swamps. A simple geometry of the surface water domain with one burrow was used and is shown in Figure 3(a). The depth of swamp water was set at 10 cm, the burrow width a 5 cm and the distance between opening 40 cm. These parameters are consistent with the range of field observations of Aucan and Ridd (2000) and Stieglitz *et al*. (2000*b*). The depth of the burrow is initially set at 20 cm, which corresponds to a burrow

(e)
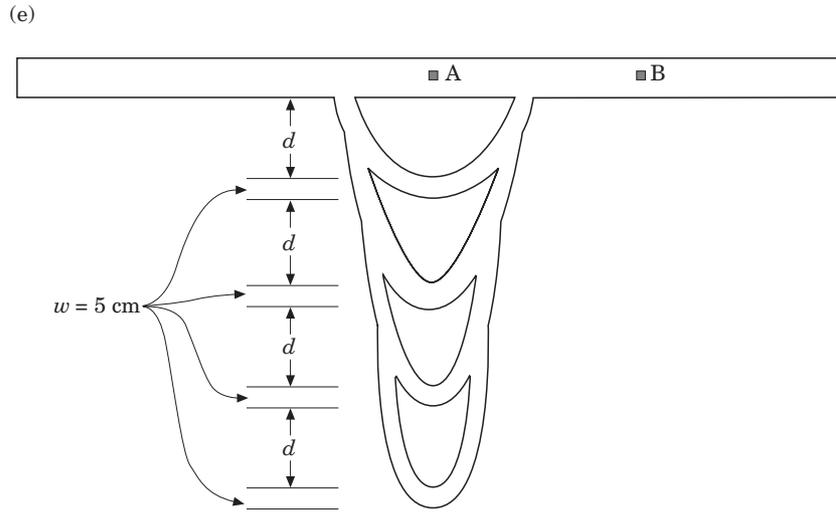
FIGURE 3 (e).

FIGURE 3. Burrow geometries, flow direction left to right. (a) Flow domain with single burrow; (b) flow domain showing alternative root positions in surface water. A: root between openings; B: root downstream; (c) buttress root of height, h, in flow domain; (d) two-burrow system; (e) four-burrow system.
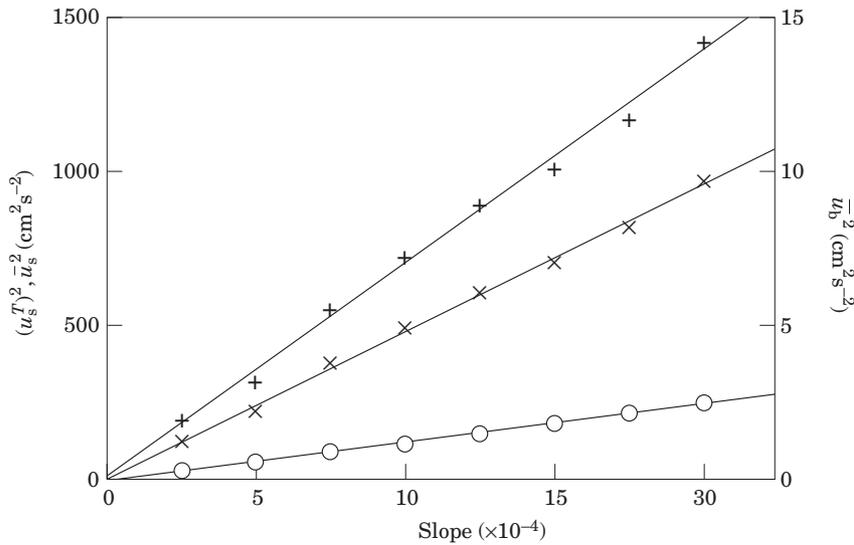
FIGURE 4. Inflow surface velocity ($\times$, $\overline{u}_s$), mean surface velocity (+, u_s^T [LH vertical scale] and mean burrow velocity ($\bigcirc$, $\overline{u}_b$ [RH vertical scale] squared plotted against water surface slope.

length of 59 cm. The inflow boundary stress condition was varied corresponding to water slopes of 1×10^{-4} to 8×10^{-4}. The velocity at the top of the surface, u_s^T; the vertically-averaged surface velocity, $\overline{u}_s$; and the mean burrow velocity, $\overline{u}_b$; are squared and plotted against water slope in Figure 4. The quadratic variation for this turbulent case contrasts with a linear variation for the laminar case (Street *et al.*, 1996). As previously stated, the water slope in mangrove swamps is generally 10^{-4} and this value is used for

the remaining studies. The velocities corresponding to this slope were $u_s^T = 13 \cdot 9$ cm s^{-1}, $\overline{u}_s = 11 \cdot 3$ cm s^{-1}, and $\overline{u}_b = 0 \cdot 6$ cm s^{-1}.

From Figure 4 we can also see that there is a linear relation between u_s^T and $\overline{u}_s$, as expected from a developed profile. The highest surface water velocities are $1 \cdot 2$ times the mean values. The mean surface velocity was used for the remaining studies due to the presence of flow obstructions (roots) in the surface water. Due to upstream effects, the roots may not
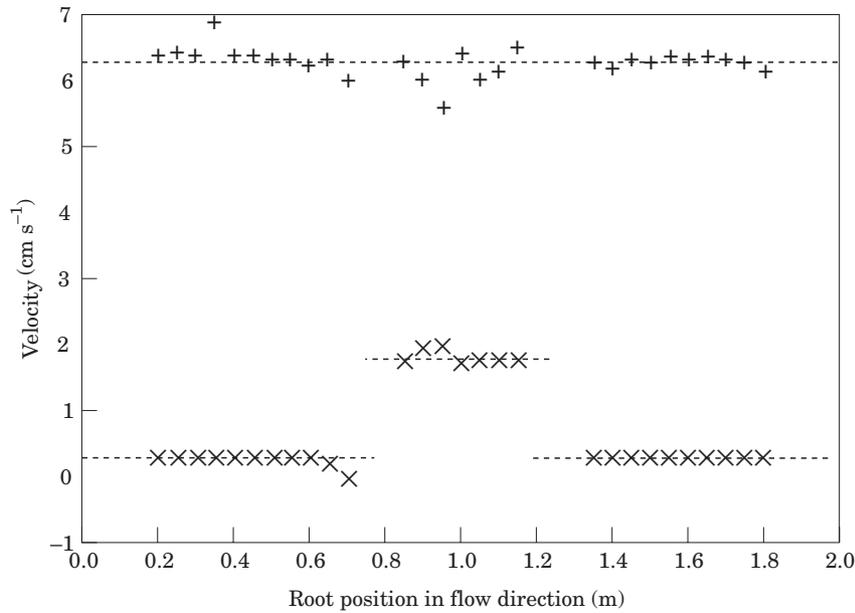
FIGURE 5. Mean surface velocity ($+$) and mean burrow velocity ($\times$) plotted against root position in the surface flow domain.

allow a true vertical profile to develop and hence the mean velocity gives a better representation of the surface flow.

Roots in surface flow

The friction to the surface flow due to the presence of roots was investigated. One root with square cross-section of side length 2 cm was placed in varying positions along the burrow direction [see Figure 3(b), roots marked as A and B] to determine the variation in the surface and burrow velocities. The square shape of the root, while chosen for computational efficiency, does not significantly alter the flow as compared with circular cross-section root. Actual root cross-sections are randomly shaped. Figure 5 shows the variations in mean surface and mean burrow velocities with position of the root relative to the burrow. The mean surface velocity is approximately constant for root locations throughout the flow domain with an average value of $\overline{\boldsymbol{u}}_s = 6 \cdot 28$ cm s^{-1}. This is a 45% reduction from the non-obstructed flow velocity given previously. The mean burrow velocity is near constant when the root is positioned either upstream or downstream of the burrow, with an average value of $\overline{\boldsymbol{u}}_b = 0 \cdot 27$ cm s^{-1} (50% reduction). However, if the root is located between the burrow openings the mean burrow velocity is increased to $\overline{\boldsymbol{u}}_b = 1 \cdot 79$ cm s^{-1}. This is due to the creation of a high pressure region upstream of the root, and a low pressure region immediately downstream of the root (see Figure 6). This pressure difference causes additional flow

through the burrow. Hence there is now a second mechanism by which the burrow flow may be increased. With the root located just upstream of the burrow, the burrow velocity is observed to tail off and becomes negative; i.e. the burrow flow is in the opposite direction to the surface flow. This flow reversal is due to the low pressure region immediately downstream of the root that is of a lower pressure than the slope-induced pressure at the downstream burrow opening. The positions of obstructions with respect to burrow openings will, in general, have a great effect on the burrow flow characteristics. The remaining studies were undertaken with one root located half way between the burrow openings [A in Figure 3(b)], and repeated with the root located downstream of the burrow at three-quarters of the domain length [B in Figure 3(b)].

Buttress root at burrow opening

A second obstruction was added to the flow domain, representing a buttress root. The buttress, of width 3 cm, was positioned downstream of the upstream burrow opening [Figure 3(c)]. The model was solved for varying buttress heights, and results are shown in Table 1. Flushing rates are determined by an advection-diffusion analysis where the burrow has an initial tracer concentration of unity. The flushing time is defined when the tracer concentration in the burrow fell to 1% of its initial value. The buttress root has a region of high pressure on its upstream side (and low pressure downstream) which increased in magnitude
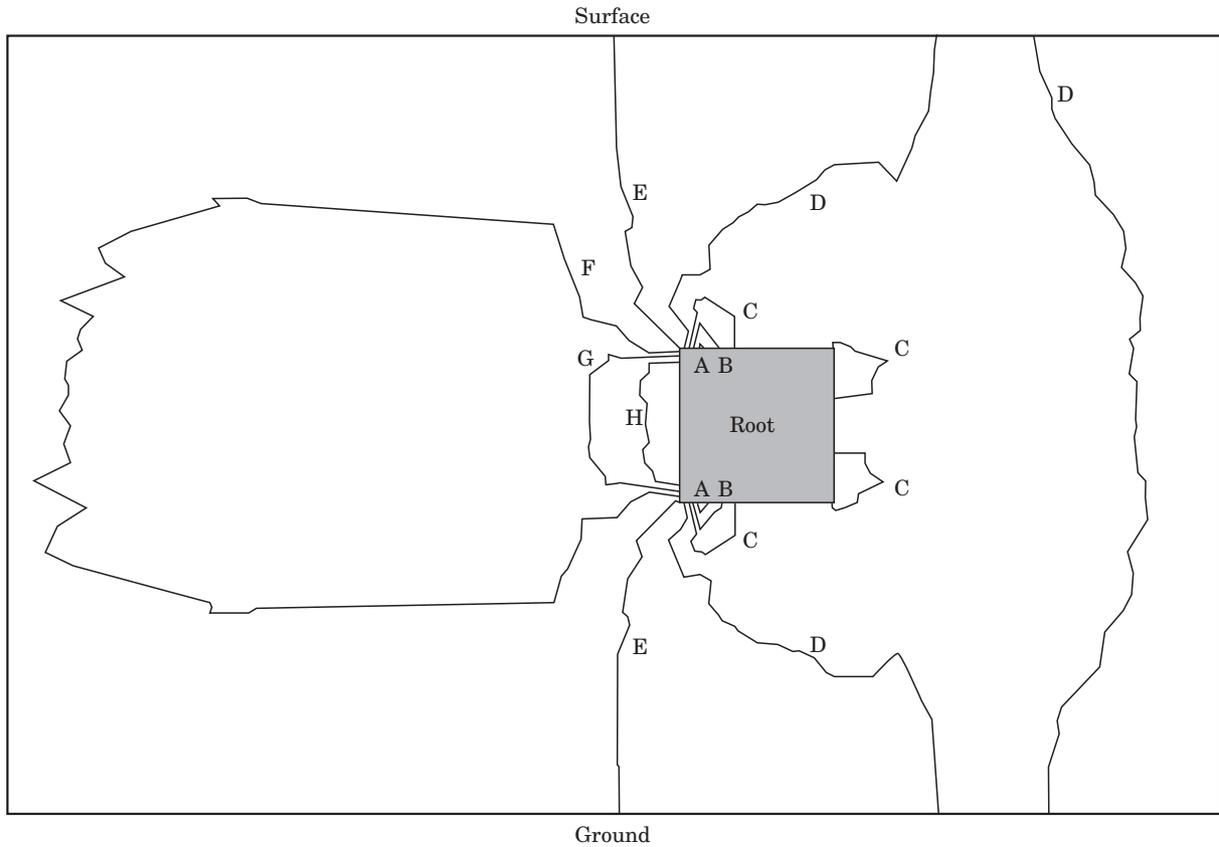
FIGURE 6. Pressure contour plot around a root in the surface water, showing the pressure increase upstream (left), and the pressure decrease downstream (right), due to the root. A: -25; B: -15; C: -5; D: 5; E: 15; F: 25; G: 35; H: 45 (dimensionless pressure units).

TABLE 1. Variation in $\overline{u_s}$; $\overline{u_b}$; and flushing time (t) for varying buttress root height (h)

	Root between openings			Root downstream		
h (cm)	$\overline{u_s}$ (cm s^{-1})	$\overline{u_b}$ (cm s^{-1})	t (min, s)	$\overline{u_s}$ (cm s^{-1})	$\overline{u_b}$ (cm s^{-1})	t (min, s)
0	6·43	1·70	1′09″	6·30	0·25	3′50″
2	6·24	2·04	0′57″	5·52	0·98	2′91″
4	5·24	2·73	0′42″	4·67	1·99	1′00″
6	4·17	3·30	0′38″	4·27	2·91	0′43″

with buttress height. The enhanced pressure difference between the burrow openings leads to an increase in burrow velocities and thus smaller flushing times. It can be seen from Table 1 that the presence of a 6 cm high buttress root can reduce the flushing times by at least a factor of 2.

Burrow depth

The depth, d, of the simple burrow was varied to determine the effect on the flushing rate of the burrow

[geometry shown in Figure 3(b)]. Stieglitz *et al.* (2000*b*) reported that the depth of burrows could be as much as 1·2 m below the swamp surface. For total flushing of a burrow this would correspond to a fluid path with a minimum length of 2·4 m. The flushing times were determined for when the burrow tracer concentration fell to 1% of the initial value. The burrow depth is varied and burrow lengths, velocities and flushing times are calculated [for a surface root positioned at A and B in Figure 3(b), respectively]. These values are shown in Table 2. As the burrow

TABLE 2. Variations in approximate burrow length (*l*) $\overline{u_b}$; and flushing time (*t* with burrow depth (*d*)

d (cm)	*l* (cm)	Root between openings		Root downstream	
		$\overline{u_b}$ (cm s^{-1})	*t* (min, s)	$\overline{u_b}$ (cm s^{-1})	*t* (min, s)
20	60	1·70	1'09"	0·25	3'50"
40	95	1·49	1'44'	0·20	7'33"
60	130	1·32	2'22"	0·18	12'10"
80	170	1·18	3'11"	0·17	17'08"
100	205	1·07	4'05"	0·17	22'33"
120	245	0·97	5'07"	0·16	28'28"

TABLE 3. Variations with depth of upper (*d1*) and lower (*d2*) burrows: *l*: approximate maximum path length; $\overline{u_b}$: mean flow at burrow opening; $\overline{u_{b1}}$: mean flow at lowest point of upper burrow; $\overline{u_{b2}}$: mean flow at lowest point of lower burrow; *t*: flushing time

d1 (cm)	*d2* (cm)	*l* (cm)	$\overline{u_b}$ (cm s^{-1})	$\overline{u_{b1}}$ (cm s^{-1})	$\overline{u_{b2}}$ (cm s^{-1})	*t* (min, s)
(a) Root between burrow openings						
20	30	130	1·83	1·48	0·35	5'22"
20	50	170	1·80	1·48	0·32	8'03"
20	70	205	1·78	1·51	0·27	11'18"
20	90	245	1·78	1·53	0·25	15'35"
40	70	245	1·57	1·24	0·33	10'04"
60	50	245	1·43	1·09	0·34	7'59"
80	30	245	1·30	1·01	0·29	6'59"
(b) Root downstream of burrow openings						
20	30	130	0·25	0·20	0·05	13'03"
20	50	170	0·25	0·21	0·04	19'49"
20	70	205	0·25	0·22	0·03	28'21"
20	90	245	0·25	0·22	0·03	38'36"
40	70	245	0·23	0·20	0·03	37'14"
60	50	245	0·21	0·18	0·03	35'54"
80	30	245	0·19	0·16	0·03	34'57"

depth is increased the total friction to the flow is increased, thus decreasing the velocities, and the burrow length is increased. The decreased velocity and increased length combine to increase the flushing time of the burrow. The effect of root position on the flushing rates can be seen to increase the flow by a factor of approximately 5.

Multiple burrows

The values in Table 2 are representative of the actual flushing times; however, the burrow structures are much more intricate than the single burrow used for these models. To determine the influence of multiple burrows a second burrow (initiating and terminating from the first burrow) was added to the model [see Figure 3(d)]. As previously, the burrow openings have separation distance of 40 cm and burrow width, *w*, of 5 cm. The upper burrow has depth, *d1*, and the lower

burrow depth, *d2*. The pressure difference across the lower burrow is much less than that across the burrow openings and produces a smaller flow rate. Table 3(a) shows the variation of flow descriptors with burrow depths for root position between burrow openings. While the addition of a second burrow may suggest a faster flow rate, the increase in surface-area-to-volume ratio of the burrow system increases the resistance to flow, thus decreasing the velocities in the entire domain. With *d1* held constant, the increase of *d2* slowed the total flow into the burrow system $\overline{u_b}$, and increased the upper burrow flow, $\overline{u_{b1}}$. The flushing time for the burrow system has a higher dependence upon the (slower) flow in the lower burrow, $\overline{u_{b2}}$, and so is significantly increased compared with Table 2 results for similar path lengths.

The total burrow depth, and thus the approximately maximum path length, of the burrow system was then held constant, the relative depths of upper and lower

TABLE 4. Variations with depth of four-burrow system: $\overline{u_b}$: mean flow at burrow opening; $\overline{u_{b1}}$, $\overline{u_{b2}}$, $\overline{u_{b3}}$, $\overline{u_{b4}}$: mean flow at lowest point of burrows 1–4, respectively; t: flushing time of burrow system

Root position	d (cm)	$\overline{u_b}$ (cm s^{-1})	$\overline{u_{b1}}$ (cm s^{-1})	$\overline{u_{b2}}$ (cm s^{-1})	$\overline{u_{b3}}$ (cm s^{-1})	$\overline{u_{b4}}$ (cm s^{-1})	t (min, s)
A	20	1·80	1·36	0·31	0·11	0·01	20′00″
	25	1·76	1·29	0·33	0·13	0·01	24′09″
B	20	0·20	0·15	0·037	0·0090	0·0005	35′10″
	25	0·21	0·17	0·037	0·0086	0·0004	47′32″

burrows varied. The flushing time decreased as *d1* is increased, due to the higher velocity in the upper burrow (compared with $\overline{u_{b2}}$), and shorter length of the lower burrow.

Table 3(b) shows the results with the root position downstream of the burrow openings. With *d1* held constant (at 20 cm) the flushing times are 2·5 times greater than in Table 3(a). These results are of the same order as the downstream results of similar path length shown in Table 2. The deviation from the single burrow values increases with *d2*, showing the high dependence of the flushing time on the lower burrow length.

To continue this investigation, a four burrow system was constructed, as shown in Figure 3(e). This geometry was selected to represent burrows similar to those of the *Sesarma messa* in Rhizophora forests, observed by Stieglitz *et al.* (2000*b*) to have bifurcations at approximate depth intervals of 20–30 cm. The burrow width was defined as 5 cm for all burrows and the model was run for burrow depths of *d*=20 cm and 25 cm (total depths 1 m and 1·2 m, respectively). The velocities and flushing times are shown in Table 4. The flushing times have increased significantly compared with two burrow systems of similar path length.

As the burrows have become more complex the flushing times have significantly increased. The increased geometric complexity and effect of burrow wall friction in 3D burrows suggests that the flushing times will again increase. As suggested for the validation of the Allanson *et al.* (1992) results, the velocities calculated may be greater than actual values due to differences in roughness characteristics in the burrow and their smaller effect due to the 2D geometry. This would suggest calculated flushing times would be less than actual values.

Conclusion

This work is the first application of computational fluid dynamics in the tidal flushing of animal burrows, and has provided a technique by which we can numerically study these flows. Investigations into various burrow geometrics were undertaken to simulate their effects on water flow and flushing times. The flushing times calculated, while likely to underestimate actual values, were of the same order as those observed for burrows in mangrove swamps (Stieglitz *et al.*, 2000*b*; Hollins & Ridd, submitted). Using this method we can investigate additional characteristics of burrow flushing, including density effects (i.e. burrow water more dense than tidal water), and further simulate the flushing properties of animal burrows using 3D models.

References

Allanson, B. R., Skinner, D. & Imberger, J. 1992 Flow in prawn burrows. *Estuarine, Coastal and Shelf Science* **35,** 253–266.

Aucan, J. & Ridd, P. V. 2000 Tidal asymmetry in creeks surrounded by salt flats and mangroves with small swamp slopes. *Wetlands Ecology and Management* **8,** 223–231.

Bode, L., Mason, L. B. & Middleton, J. H. 1997 Reef parameterisation schemes with applications to tidal modelling. *Progress in Oceanography* **40,** 285–324.

Fluid Dynamics International 1993 *Fluid Dynamics Analysis Package v7.0 Theory Manual*. FDI, Evanston, Illinois.

Furukawa, K., Wolanski, E. & Mueller, H. 1997 Currents and sediment transport in mangrove forests. *Estuarine, Coastal and Shelf Science* **44,** 301–310.

Hollins, S. & Ridd, P. The concentration and consumption of oxygen in large animal burrows in tropical mangrove swamps. *Estuarine, Coastal and Shelf Science* (submitted).

Hollins, S., Ridd, P. V. & Read, W. W. 1999 Measurement of the diffusion coefficient for salt in salt flat mangrove soils. *Mangroves and Salt Marshes* **73,** 1–6.

Passioura, J. B., Ball, M. C. & Knight, J. H. 1992 Mangroves may salinize the soil and in so doing limit their transpiration. *Functional Ecology* **6,** 476–481.

Ridd, P. V. 1996 Flow through animal burrows in mangrove creeks. *Estuarine, Coastal and Shelf Science* **43,** 617–625.

Stieglitz, T., Ridd, P. & Hollins, S. 2000*a* A small sensor for detecting animal burrows and monitoring burrow water conductivity. *Mangroves and Salt Marshes* **8,** 1–7.

Stieglitz, T., Ridd, P. & Muller, P. 2000*b* Passive irrigation and functional morphology of crustacean burrows in a tropical mangrove swamp. *Hydrobiologia* **421,** 69–76.

Street, R. L., Watters, G. Z. & Vennard, J. K. 1996 *Elementary Fluid Mechanics*, 7th Edition. John Wiley & Sons, Inc., New York, 757 pp.

Tomlinson, P. B. 1986 *The Botany of Mangroves*. Cambridge University Press, Cambridge, 413 pp.

Webster, I. T. 1992 Wave enhancement of solute exchange within empty burrows. *Limnology and Oceanography* **37,** 630–643.

Wolanski, E. & Ridd, P. 1986 Tidal mixing and trapping in mangrove swamps. *Estuarine, Coastal and Shelf Science* **23,** 759–771.

Wolanski, E., Mazda, Y. & Ridd, P. 1992 Mangrove Hydrodynamics. In *Tropical Mangrove Ecosystems* (Robertson, A. & Alongi, D., eds), American Geophysical Union, Washington DC, pp. 43–61.